16.32 Optimal Control and Estimation

Term Project

Optimization of Propellant Mass Fraction for High Mass Mars Entry, Descent and Landing

Author:
Jessica Todd

Professor:
Prof. Steven Hall

4 May 2020

1 Nomenclature

β = Ballistic Coefficient, km/m^2
A = vehicle reference area, m^2
C_D = Drag Coefficient
L/D = Lift to Drag Ratio
L = Lift, N
D = Drag, N
h = altitude, km
v = velocity, km/s
γ = flight path angle, deg
m = entry vehicle mass, kg
σ = bank angle, deg
ψ = heading, deg
θ = longitude, deg
r = distance from centre of Mars, km
phi = latitude, deg
T = thrust, N
s = downrange distance, km
Isp = specific impulse, s
r_n = nose radius, m
rho = atmospheric density, kg/m^3
n = G-loading
$\dot{q}$ = convective heat rate, W/cm^3

2 Introduction

Mars entry, descent and landing (EDL) is a challenging problem. The goal of any EDL system is to dissipate a sufficient amount of energy during atmospheric entry and descent to safely land a payload at low speeds, at an appropriate altitude, and within a certain landing ellipse. However the Martian atmosphere and terrain pose significant challenges when designing an EDL system that can decrease the high entry velocities from a Mars or transit orbit. The Mars atmosphere is thick enough to generate significant heating during entry however its low density (approximately 1/100th Earth atmospheric density) and the planet's comparatively high gravity (approximately 1/3 Earth gravity) means the atmosphere is far less effective at slowing a spacecraft during entry and descent.[1] Currently all Mars EDL systems are heavily reliant on aerodynamic forces to slow the vehicle through the atmosphere, and utilise additional systems such as parachutes, airbags, and retropropulsion to further dissipate energy.[2] However to date, the largest landed mass on Mars is the 900kg Curiosity rover, as part of the Mars Science Laboratory (MSL) mission. The EDL systems used by this mission were operating at the limit of their payload mass capability, and landing anything larger on the surface necessitates a redesign of traditional Mars EDL.

NASA's current human exploration roadmap aims to land humans on Mars in the 2030s, and the constraints of such a mission pose unique challenges for future EDL systems, including

- **Higher mass requirements**. The NASA Design Reference Architecture 5.0 estimated the mass of human-class payloads required for sustained surface exploration of Mars is between 40 and 80 tonnes,[3] including habitation and life-support systems, transport vehicles, power generation, and in-situ resource utilization infrastructure.
- **Greater precision in landing** to ensure cargo and crew do not have to traverse. MSL landed within a 20km ellipse, however crewed and cargo descent vehicles will need to land with accuracy on the order of tens of meters.
- **Stricter loading requirements** on crewed descent vehicle, with g-forces not exceeding 4.5-5 g's.

This project aims to optimize a Mars entry control scheme for a crewed descent vehicle, with the goal to *maximize the landed payload mass* using supersonic retropropulsion systems, a proposed EDL technology for human exploration missions. To address the additional challenges listed above, a control scheme was selected that allows for precision landing while ensuring the descent vehicle remains below the maximum load factor and within the heating bounds of the spacecraft. The optimization problem was implemented into the MATLAB GPOPS-II software,[4] and run for a number of different initial conditions. This report outlines the reference vehicle, control scheme and dynamics modelled, the implementation into the GPOPS-II software, and results of the optimization.

3 Historical Context and Problem Scope

NASA has successfully landed 8 payloads on the Martian surface, however current EDL technology is near the limit of its landed mass capability.[1] The Mars Science Laboratory system represents the state-of-the-art in EDL. During the initial hypoersonic phase of entry and descent the MSL aeroshell achieved the majority of the deceleration, slowing the vehicle to low supersonic speeds. Unlike previous Mars missions, it employed a guided entry trajectory, utilising bank angle control during this hypersonic descent phase (similar to the control scheme used for the Apollo re-entry phase).[5] Like previous missions, once the entry vehicle (EV) had been slowed sufficiently, a supersonic parachute was deployed to further slow the vehicle during the supersonic phase, and finally a novel retropropulsion system and skycrane was used to safely deposit the Curiosity rover on the surface.

As highlighted above, the key issue with human exploration missions to Mars is the increased landed mass requirement, which is captured in the ballistic coefficient of the vehicle. Two key metrics for examining EDL are the lift-to-drag $\frac{L}{D}$ ratio of the EV, and the ballistic coefficient β of EV

$$\beta = \frac{m}{C_D A} \tag{1}$$

where m is the mass of the vehicle, C_D is the drag coefficient and A is the reference area. The entry system's heating profile and deceleration through the atmosphere is governed by the ballistic coefficient. As landed mass increases, the diameter of the EV must also increase to keep the ballistic coefficient as low as possible. A higher ballistic coefficient means the EV penetrates deeper into the atmosphere before it decelerates, meaning parachutes must be deployed at either very high velocities, or at very low altitudes which may not leave sufficient time for the craft to decelerate. A selection of previous Mars missions has been highlighted in Table 1 to illustrate the changes in terminal altitude and velocity (the altitude and velocity at which parachutes are deployed), landed mass and ballistic coefficient. MSL's record-breaking 20m diameter parachute was deployed at Mach 2.2 and there is no current way of surpassing

this limit with a stable parachute at higher velocities for a greater mass. A ballistic coefficent of 125kg/m^2 or greater exceeds the supersonic deployment region for parachutes.[1]

Consequently, a high-mass Mars lander for a human exploration mission will need to employ alternative EDL methods for safe landing. In order to lower the ballistic coeffcient, a deployable or inflatable aeroshell that increases the EV diameter without drastically increasing the mass could be used. This system would allow the EV to remain inside the supersonic deployment region for parachutes. Alternatively, a supersonic retropropulsion system (SRP) could be used to slow the EV during the supersonic phase of the descent. While being less mass efficient than a deployable aeroshell, SRPs would be much less suseptible to atmospheric uncertainties and perturbations during descent. Additionally they allow for a higher degree of control at supersonic speeds and make the system fully controllable throughout all phases of the landing. Finally, the SRPs allow for greater landing precision than a parachute, a key requirement of human EDL systems.

This study examines the use of SRPs for EDL. Following a bank-angled controlled descent through the Martian atmosphere, similar to the MSL descent, SRPs can be deployed at Mach 3 to sufficiently slow the craft for landing. Performance is evaluated on the ability of the EDL system to deliver a high mass payload to the surface. As SRPs rely on propellant for deccelleration, this study aims to maximise the possible landed mass achievable and thus determine the minimum possible propellant mass fraction, *PMF*.

Table 1: Past successful NASA Mars EDL Missions[1]

Mission	**Viking 1**	**Mars Pathfinder**	**MER-A (Spirit)**	**MSL**
Year	1976	1997	2004	2010
Entry from	Orbit	Direct	Direct	Direct
Entry v (km/s)	4.7	7.26	5.4	5.5
β (km/m^2)	64	63	94	115
Entry m (kg)	992	584	827	2920
Entry AoA Trim (\degree)	-11	0	0	-15
Entry Guidance	Unguided	Unguided	Unguided	Apollo Guidance
L/D	0.18	0	0	0.24
Peak Heating (W/cm2)	26	100	44	<210
Terminal Velocity (Mach)	1.1	1.57	1.77	2.2
Terminal Altitude (km)	5.79	9.4	7.4	6.5
Descent Attitude Control	RCS Roll Rate	None	None	RCS Roll Rate
Touchdown Mass (kg)	590	360	539	1590
Useful Landed Mass (kg)	244	92	173	800
3σ Landing Ellipse Axis (km)	280 (maj), 100 (min)	200 (maj.), 100 (min.)	80 (maj.), 12 (min)	20 (maj.), 20 (min.)

4 EDL Formulation

The EDL problem is similar to that of previous Mars missions. After entering the Martian atmosphere at an altitude of 125km, the entry vehicle (EV) follows a ballistic trajectory towards the surface in what is referred to as the *unpowered phase*, relying only on atmospheric lift and drag for deceleration using bank-angle control. This is followed by the *powered phase*, where thrust from SRPs is used for further deceleration and no bank-angle control is permitted. The EDL formulation is terminated just above the surface, as soft landing rockets for the final touchdown were not modelled in this simulation.

5 Reference Missions

The study considers entry into the Martian atmosphere from orbit using an aercapture maneouvre. A direct entry from a hyperbolic approach trajectory was used by MSL, MERS and Pathfinder, with an entry velocity of $\sim$5.85 km/s. However in order to minimize transit time between Earth and Mars, a crewed vehicle would likely arrive at Mars travelling considerably faster than previous Mars missions and so a second entry from orbit was considered. This assumes that an aerocapture maneouvre was used to place the EV at a lower entry velocity

of 3.36 km/s, entering the atmosphere at a 125km altitude. Figure 1 highlights the difference between the two entry trajectories.

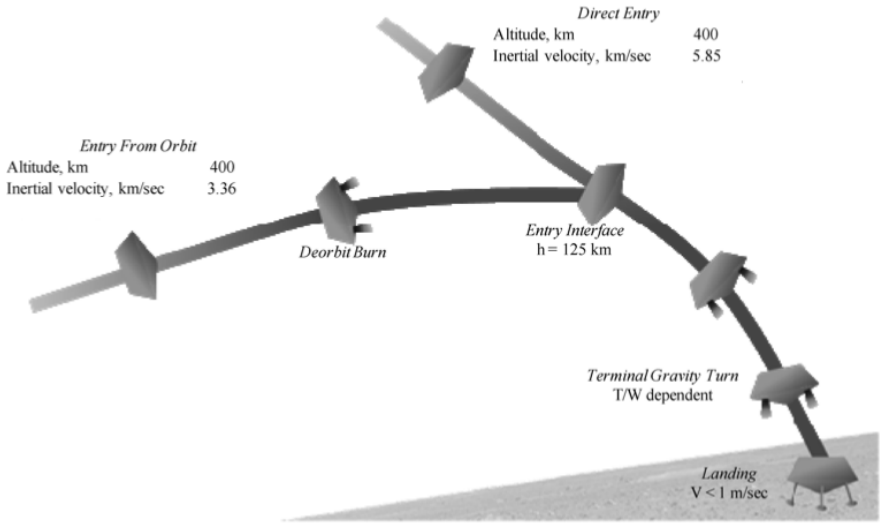

Figure 1: EDL sequence of events for two reference missions[6]

5.1 Entry and Unpowered Descent Phase

Control during the hypersonic unpowered descent phase is given by rolling the descent vehicle to alter the lift vector. This is achieved by changing the bank angle σ of the EV. The equations of motion for a body entering an atmosphere are given below[7]

$$\dot{h} = v \sin\gamma \tag{2}$$

$$\dot{v} = \frac{-D}{m} - g \sin\gamma \tag{3}$$

$$\dot{\gamma} = \frac{L \cos\sigma}{mv} - \frac{g}{v} \cos\sigma + \frac{v}{r} \cos\gamma \tag{4}$$

$$\dot{\psi} = \frac{L \sin\sigma}{mv \cos\gamma} + \frac{v \cos\gamma \sin\psi \tan\phi}{r} \tag{5}$$

$$\dot{\theta} = \frac{v \cos\gamma \sin\psi}{r \cos\phi} \tag{6}$$

$$\dot{\phi} = \frac{v \cos\gamma \cos\psi}{r} \tag{7}$$

Longitudinal motion and lateral-directional motion are decoupled and thus can be treated independently. As the EV is rolled, this generates both a vertical and horizontal lift component. The horizontal lift component increases the cross-range of the vehicle. For the purposes of this simulation, the EV was assumed to enter the atmosphere over the Martian equator at a latitude of 0°and longitude of 0°, and only forces acting in the longitudinal direction were considered. Thus the set of equations of motion is reduced to functions of altitude h, velocity v, flight path angle γ and downrange distance s. The coordinate frame of reference for the vehicle is shown in Figure 2.

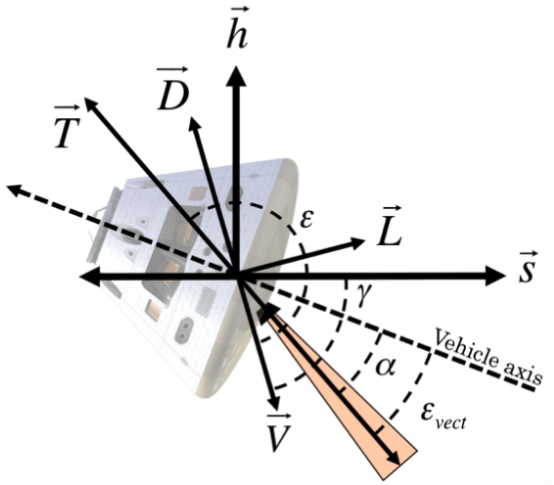

Figure 2: Relevant coordinates in the trajectory plane. For this problem, thrust is assumed to be axial and thus $\epsilon = 0$

$$\dot{h} = v \sin\gamma \tag{8}$$

$$\dot{v} = -\frac{D}{m} - g \sin\gamma \tag{9}$$

$$\dot{\gamma} = \frac{L \cos\sigma}{mv} - \frac{g}{v} \cos\sigma + \frac{v}{r} \cos\gamma \tag{10}$$

$$\dot{s} = \int \dot{\theta} = v \sin\gamma \tag{11}$$

As L and D are dependent on angle of attack, and angle of attack was kept constant during EDL, the equations of motion can be written in terms of the descent vehicles L/D_{max} and ballistic coefficent $\beta = \frac{m}{C_D A}$.

$$\dot{h} = v \sin\gamma \tag{12}$$

$$\dot{v} = -\frac{\rho v^2}{2\beta} - g \sin\gamma \tag{13}$$

$$\dot{\gamma} = \frac{\rho v}{2\beta} \left(\frac{L}{D_{max}} \right) u_\sigma - \frac{g}{v} \cos\gamma + \frac{v}{r} \cos\gamma \tag{14}$$

$$\dot{s} = v \sin\gamma \tag{15}$$

The state variables are

$$\mathbf{x} = [h, v, \gamma, s]^T \tag{16}$$

The spacecraft was controlled using bank angle modulation

$$u_\sigma = \cos\sigma \in [-1, +1] \tag{17}$$

The relationship between bank angle and the lift-to-drag ratio can be seen in Figure 3.

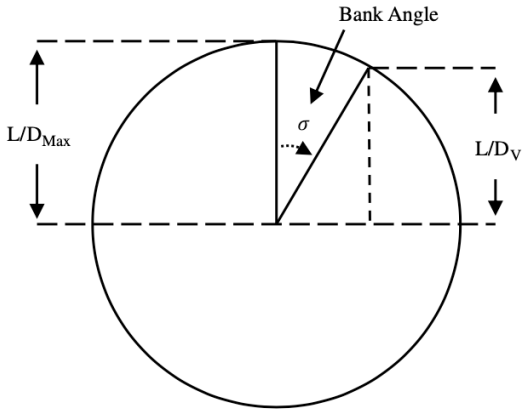

Figure 3: Geometry of vertical L/D ratio for a bank-angle-controlled entry vehicle. The bank angle is a positive rotation about the velocity vector[8]

5.2 Powered Descent Phase

The equations of motion for the powered descent phase are given below. The powered descent was modelled as a gravity turn, firing the SRP opposite to the velocity vector, with no bank angle control. As the vehicle loses horizontal velocity, the gravity of Mars pulls the vehicle into a vertical descent. While this delivers a near-optimal result, future Mars missions will likely employ vectored thrusting for powered descent. The SRP was assumed to have a throttle depth of 100%, as a multiengine system could achieve near 100% throttle depth similar to the MSL skycrane system.[8] The equations of motion have an additional mass rate term, to account for the change in mass due to propellant use.[8]

$$\dot{h} = v \sin\gamma \tag{18}$$

$$\dot{v} = -\frac{\rho v^2}{2\beta} - \frac{T u_T}{m} - g \sin\gamma \tag{19}$$

$$\dot{\gamma} = \frac{\rho v}{2\beta}\left(\frac{L}{D_{max}}\right)\cos\sigma - \frac{g}{v}\cos\gamma + \frac{v}{r}\cos\gamma \tag{20}$$

$$\dot{m} = -\frac{T u_T}{g_0 I_{sp}} \tag{21}$$

$$\dot{s} = v \sin\gamma \tag{22}$$

where $u_T \in [0, 1]$ is the throttle control and T is the maximum possible thrust. The state variables are

$$\mathbf{x} = [h, v, \gamma, s, m]^T \tag{23}$$

5.3 Constraints on Trajectories

For a crewed mission to Mars, a crucial constraint is the g-loading on the EV. During Apollo missions, astronauts experienced up to 9 g's however space shuttle missions sought to restrict that to 3 g's. For the ballistic trajectory and subsequent powered descent through the Martian atmosphere, the maximum allowable g-forces have been set to 4.5 g's, with G-loading on the

vehicle given as

$$n = \frac{\sqrt{L^2 + D^2}}{mg} \tag{24}$$

$$= \frac{\rho v^2}{2\beta g}\sqrt{\left(\frac{L}{D}\right)^2 + 1} \tag{25}$$

The other important constraint for entry trajectories is convective heat-rate on the vehicle. The maximum allowable heat rate is determined by the vehicle and heat shield properties and was limited to 100 W/cm^3. The convective heat rate is given by the Sutton-Graves heating law[9]

$$\dot{q} = k\sqrt{\frac{\rho}{r_n}}v^3 \tag{26}$$

where k for Mars is given below, and the reference nose radius r_n for the Orion reference vehicle is 6.1 m at low angles of attack ($< 25°$).[10]

5.4 Atmospheric and Gravity Model

The standard design approximations of an exponential graph are less accurate for a Martian atmosphere than an Earth atmosphere (due to $\pm 20\%$ annual change in pressure and density due to sublimation of the south pole during summer). However since precise estimates of atmospheric density aren't essential for gaining an understanding of the effect of thrust and bank angle control on landing, a standard exponential model based on yearly average density is sufficient for this study,ignoring effects of Martian wind.

$$\rho = \rho_0 e^{\left(\frac{h_0 - h}{H}\right)} \tag{27}$$

The study also assumed a point mass gravity model, with a spherical Mars based on the Martian radius at the equator.

Table 2: Martian Constants

Parameter	**Variable**	**Value**
Acceleration due to gravity	g_0	3.71 m/s^2 [11]
Reference Density	ρ_0	0.02 km/m^3 [11]
Reference Altitude	h_0	0 km [11]
Equatorial Radius	r_E	3397 km [11]
Atmospheric Scale Height	H	11.1 km [11]
Standard Gravitational Parameter	μ	42828.371901 km^3/s^2
Sutton-Graves Constant (Convective heating)	k	1.9027e-4 $\sqrt{\text{kg}}$/m [12]

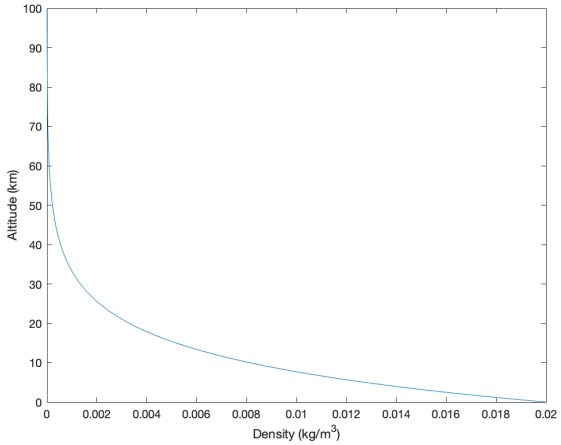

Figure 4: Standard exponential model of the Martian Atmosphere. A vacuum is assumed beyond an altitude of 100km.

5.5 Reference Vehicle

The reference crew vehicle was assumed to be a derivative of the crewed Orion capsule. As is the case with all previous Mars surface missions, the entry vehicle (EV) employs a 70°sphere cone aeroshell, using aerodynamic forces to stabilise the vehicle to a fixed attitude (angle of attack). The vehicle would be packaged to offset the center-of-mass to achieve the vehicle's desired trim. Drag forces are used to reduce the vehicle's velocity, and lift forces control the descent rate through the atmosphere. As was the case with the MSL and the Apollo command module, the Mars EV is controlled by a reaction control system that rotates the vehicle relative to the velocity vector to achieve a desired bank angle, thereby altering the vertical lift component.[13] A heavier cargo vehicle was also considered, drawing on the reference values of the Orion capsule, but with a great mass, diameter and beta coefficient.The nominal parameters for the reference crew vehicle and cargo vehicle are given in Table 3 The Mars Science Laboratory has been included for comparison. A variety of L/D ratios were examined, 0.15, 0.25, 0.35, and 0.5. For comparison, the MSL has a L/D of 0.24, the Apollo capsule has a L/D of 0.35 and the peak L/D value for the Orion Capsule is 0.63.[2]

Table 3: Nominal vehicle parameters for Mars Entry Vehicles

Parameter	**Orion**[2]	**Cargo Orion**[6]	**MSL**[5]
Aeroshell Diameter	6.1 m	10 m	4.5 m
Entry Mass	10,400 kg	40,000 kg	2,800 kg
Ballistic Coefficient	340 km/m^2	400 km/m^2	115 km/m^2
L/D	0.15, 0.25, 0.35, 0.5	0.15, 0.25, 0.35, 0.5	0.24

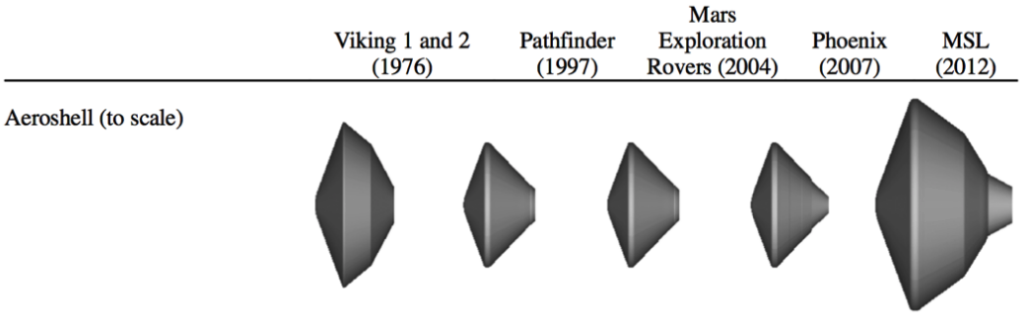

Figure 5: Examples of 70°sphere cones used in previous Mars EDL

5.6 Supersonic Retropropulsion System

In exploring SRPs as a powered descent method, two different propellant systems were examined to see the effect of I_{sp} on landed mass capability. Future Mars missions will likely use a LOX-Methane fuel source, as methane can be readily produced from the Martian atmosphere and thus it is easier to refuel and relaunch a vehicle.[2] The LOX-Methane SRP explored is a theoretical SRP system described in.[14] However LOX-Methane is difficult to cryogenically store for long periods of time, such as during the 8 month transit from Earth to Mars, and will likely not be used as a fuel source until there are ISRU capabilities on Mars. Consequently a heritage SRP system was also examined, the SpaceX SuperDraco engines, which employ a hypergolic bipropellant. The smaller Draco engine has been succesfully demonstrated in flight, landing the Falcon 9 first stage. Maximum axial thrust was kept constant across both systems, as it is assumed mutliple engines could be used to achieve desired thrust. Throttle depth was assumed to be 100% as a multiengine system could achieve near 100% throttle depth similar to the MSL skycrane system by toggling different engines.[8]

Engine	**Fuel**	**Number of Engines**	$\mathbf{I_{sp}}$	**Total** $\mathbf{T_{axial,max}}$
Draco	N_2O_4 - Hydrazine	8	240 s	568,000 N
Future	LOX - Methane	2	360 s	600,000 N

6 GPOPS-II Simulation

6.1 Setup

GPOPS-II was used for this optimization simulation. ADiGator, an automatic differentiation tool, was used to speed up the solving process. Table 4 describes the solver setup.

Table 4: GPOPS-II Solver Setup

Parameter	**Value**
NLP Solver	ipopt
Derivatives Supplier	SparseCD
Derivative Level	second
Scaling Method	automatic-bounds
Method	RPM-Differentiation
Solver Option	mumps
Mesh Method	hp-PattersonRao
Mesh Tolerance	1.00E-5

6.2 Strategy

The entry, descent and landing of a crewed Mars vehicle was examined as both two single phase problems, and multiphase problem:

- Single Phase - Unpowered Descent with Bank Angle Control
- Single Phase - Powered Descent with Throtte Control
- Two Phase - Unpowered Descent with Bank Angle Control followed by Powered Descent with Throttle Control

To verify the dynamic equations and constraints, as well as gain an understanding of reasonable values for terminal altitude and velocity as well as control performance, a single phase problem was constructed for the unpowered descent. The unpowered descent simulation was optimising for terminal altitude (i.e. the altitude at which you would typically deploy a parachute, inflatable aeroshell, or supersonic retropropulsion system). The goal was to achieve the highest possible terminal altitude within the SRP supersonic range ($\sim$ Mach 3) that would allow for ignition of the SRP stage. Thus the objective function for this problem was

$$J = -h_f + \int_{t_0}^{t_f} 0.1 \cdot cos^2(\sigma(t))dt \tag{28}$$

The powered descent phase was then likewise run as a single phase, with the starting velocity and altitude taken from the results of the single phase unpowered descent optimized solution. In this phase, total landing mass was optimized

$$J = -m_f \tag{29}$$

Finally the entire EDL sequence was formulated as a two-phase problem, with the first phase using the bank angle control and a free terminal time and altitude, and the second phase using throttle control. The problem was set up so that the switch time between phases was left free and an event control was placed on the system to ensure that stats before and after the phase switch were equal. The two phase problem was optimizing for landing mass, as described in Equation 29.

Entry velocity into the Martian atmosphere was determined from the refernce missions. Terminal velocity (i.e. velocity at conclusion of unpowered descent) was selected to be supersonic for ignition of the SRP. Initial and terminal conditions, and bounds, will be highlighted in the results section. In all three cases, the path constraints for g-loading and heating rate were enforced

$$G_{max} < 4.5 \tag{30}$$

$$\dot{q} < 100 \tag{31}$$

7 Results

7.1 Single Phase - Unpowered Descent

7.1.1 Set Up

The initial and terminal values for time states and control variables are given in Table 5 and the bounds for the flight parameters given in Table 6

Table 5: Initial and Terminal Conditions for One Phase Unpowered Descent

Variable	**Initial**	**Final**
Time (s)	0	free
Altitude (km)	125	free
Velocity (km/s)	3.36	0.854
Flight Path Angle (°)	-15	free
Downrange Distance (km)	0	free

Table 6: Flight Parameter Bounds for One Phase Unpowered Descent

Variable	Lower	Upper
Time (s)	0	5000
Altitude (km)	1	125
Velocity (km/s)	0.45	7.5
Flight Path Angle (°)	-25	25
Downrange Distance (km)	-500	935
Cosine of Bank	-1	1
G-Loading	0	4.5
Heat-Rate (W/cm^2)	0	100

The results are shown in the figures below. The optimization program was run for both the Human Orion entry vehicle and the Cargo Orion EV at different L/D, as well as the nominal Mars Science Laboratory for comparison.

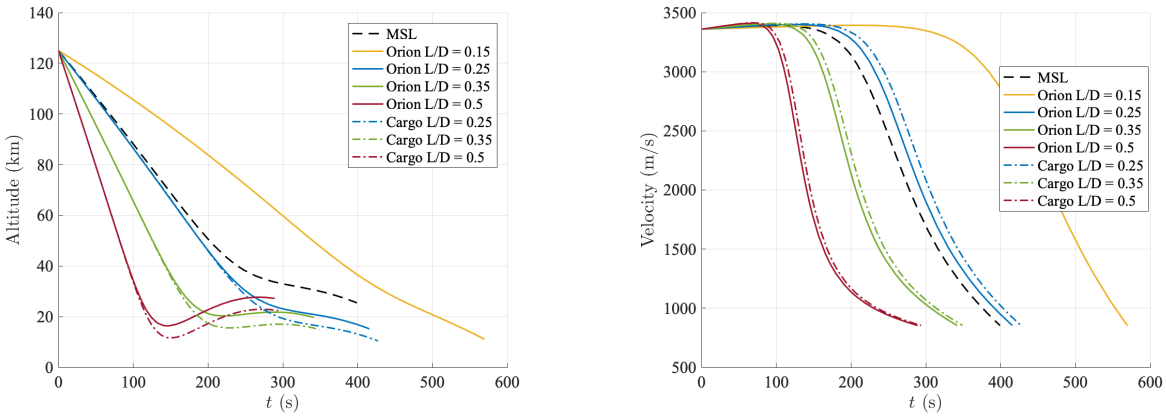

Figure 6: Altitude *(left)* and velocity *(right)* during EDL with Bank Angle Control

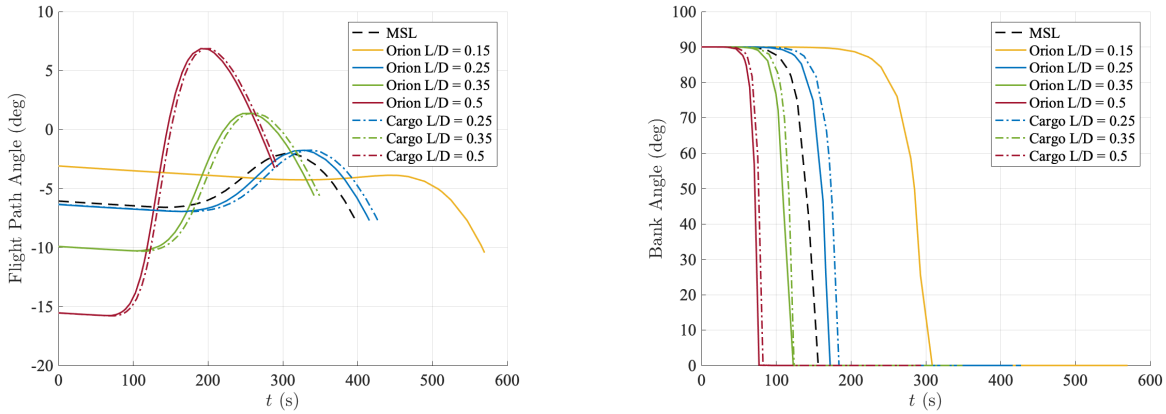

Figure 7: Flight Path Angle (*left*), and Optimal Bank Angle (*right*) during EDL with Bank Angle Control

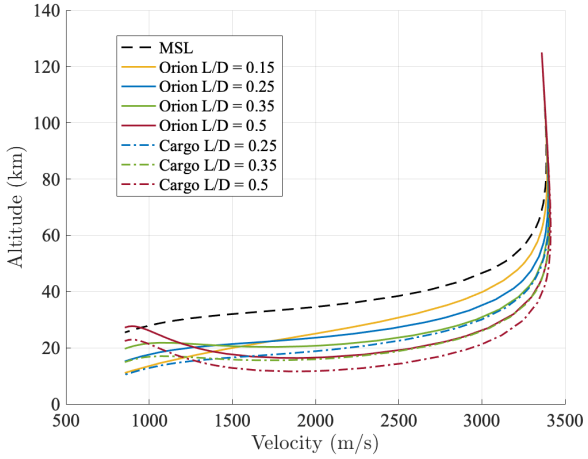

Figure 8: Altitude vs Velocity for Bank Angle Control EDL

All scenarios converged to an optimal solution except for the Cargo EV with L/D = 0.15, which reached a point of infeasibility. The bank angle control performs as expected. In all cases, the spacecraft begins with the bank angle at 90°, producing no vertical lift component and performs a single switch to a full lift-up configuration with the bank angle held at 0°. For high L/D cases, this switch occurs more rapidly and earlier in the EDL sequence, likely to take advantage of the lift vector in slowing the spacecraft. When a loading of 4.5 g's was not imposed, this switch was observed to be much more rapid and near vertical. The enforcement of a 4.5g maximum see the bank angle change become slightly more gradual. It should be noted that no restriction was placed on the angular rate or angular acceleration for the bank angle control. A high angular acceleration would induce more G's on the occupants and should be taken into consideration in future simulations.

As expected the MSL reaches terminal velocity at a much higher altitude than any of the Orion or Cargo EVs, due to its lower ballistic coefficient and higher L/D ratio. The MSL is able to dissipate its orbital velocity much more rapidly. Previous studies have shown that reaching terminal velocity at an altitude of ∼10 km is acceptable for Mars EDL in order to have sufficient altitude over which to deploy a parachute and decelerate. Interestingly, the higher L/D ratios resulted in the altitude decreasing and then increasing slightly before reaching terminal velocity. In all cases, the Orion EV reached a higher terminal altitude than the L/D equivalent Cargo EV, due it its ballistic coefficient being lower than the Cargo EV.

All scenarios result in considerable downrange distance, which increases with lower L/D. This would need to be taken into account in the entry position of the spacecraft into the atmosphere, or by incorporating downrange control.

Table 7: Terminal Altitudes and Downrange Distances for EDL

Entry Vehicle	β	**L/D**	**Terminal Altitude (km)**	**Downrange (km)**	**Flight Path Angle (°)**
MSL	115	0.24	25.46	99.54	-7.92
Orion	300	0.15	11.08	113.92	-10.44
	300	0.25	15.20	109.80	-7.72
	300	0.35	19.67	105.33	-5.6
	300	0.5	27.18	97.82	-3.26
Cargo	460	0.25	10.44	114.56	-7.73
	460	0.35	14.91	110.09	-5.61
	460	0.5	22.41	102.59	-3.27

These results show that bank angle control can be used to reach optimal terminal altitudes for deployment of SRPs or an alternative deceleration method. As the mass, and consequently

the ballistic coefficient increase the terminal altitude decreases. The EDL system must compensate by either increasing the L/D ratio, or extending the capability of the SRP system to be able to ignite at a higher supersonic speed.

7.2 Single Phase - Powered Descent

The initial and terminal values for time states and control variables are given in Table 8 and the bounds for the flight parameters given in Table 9. The initial conditions were taken from the final conditions of the single unpowered descent phase to ascertain if SRPs would be sufficient to land the EV with mass to spare. The terminal altitude and flight path angle were determined by the relevant case given in Table 7. Bank angle was held fixed at 0°.

Table 8: Initial and Terminal Conditions for One Phase Powered Descent

Variable	**Initial**	**Final**
Time (s)	0	free
Altitude (km)	Variable	0
Velocity (km/s)	854	0
Flight Path Angle (°)	-10.44	free
Downrange Distance (km)	Variable	free
Bank Angle (°)	0	0
Mass (kg)	10,400, 40,000	free

Table 9: Flight Parameter Bounds for One Phase Powered Descent

Variable	**Lower**	**Upper**
Time (s)	0	5000
Altitude (km)	1	125
Velocity (km/s)	0	7.5
Flight Path Angle (°)	-90	90
Downrange Distance (km)	-500	935
Bank Angle (°)	0	0
Mass (kg)	0	10,400, 40,000
Throttle	0	1
G-Loading	0	4.5
Heat-Rate (W/cm^2)	0	100

As the MSL descends to the surface using a combination of supersonic parachutes and subsonic retropropulsion, it was not included in this analysis. The simulation was run for the proposed LOX-Methane system. Following the simulation, select cases were run with the SpaceX SuperDraco for comparison to determine the effects of Isp.

The results of the optimization are below. Figures 9-12 show results for the LOX-Methane propellant. From the graphs it is evident that the controller switches on the SRP at the possible possible moment to conserve fuel and maximize deceleration due to atmospheric drag. The EV in fully-lift up configuration (bank angle = 0°) falls unpowered before the SRP is fired up, during which there is a steep decline in velocity. The length of this freefall varies with ballistic coefficient and L/D. The lighter Orion EV falls longer before SRP ignition, and EVs with a higher L/D wait longer to ignite SRP. As expected, the flight path angle becomes more vertical due to the gravity turn and the altitude decreases at an almost constant rate during both the freefall and the powered descent, leveling off slightly as the EV nears the ground. In all cases the throttle is quickly set to maximum once ignited, to minimize gravity losses during the descent. There is little difference in the landed mass across different L/D within each vehicle

(a difference of ∼120 kg across Orion vehicle and a difference of ∼170 kg across the Cargo vehicles).

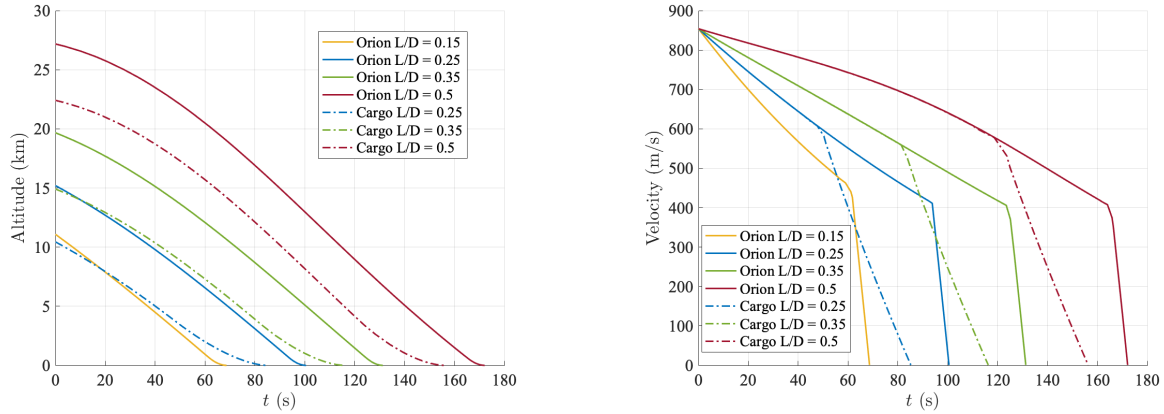

Figure 9: Altitude (*left*) and velocity (*right*) during EDL with Throttle Control

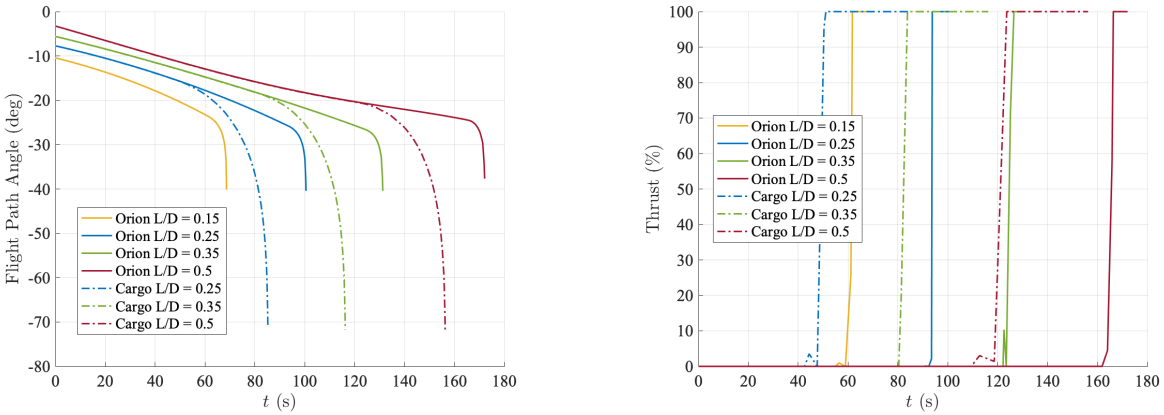

Figure 10: Flight Path Angle (left) during EDL, and Optimal Thrust (*right*) during EDL with Throttle Control

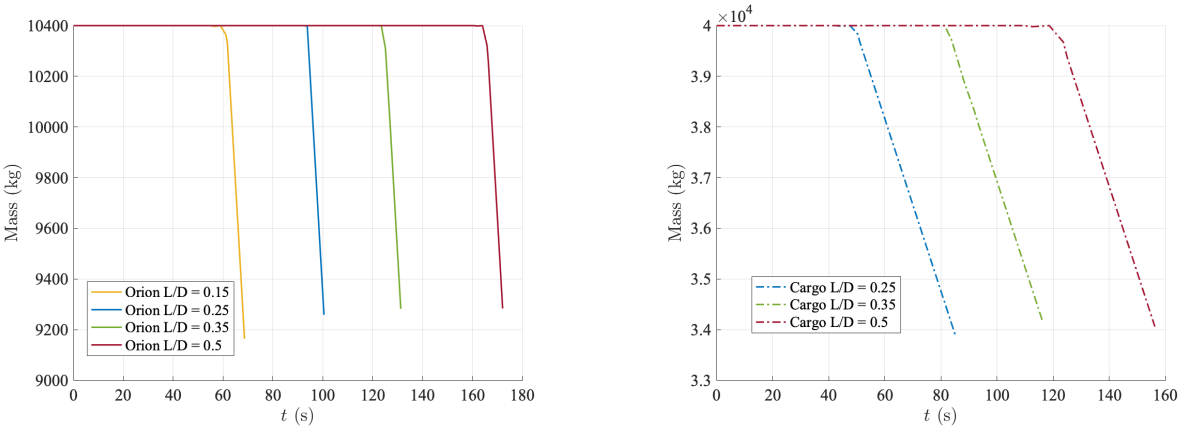

Figure 11: Mass change for Orion (*left*) and Cargo (*right*) during EDL for powered descent

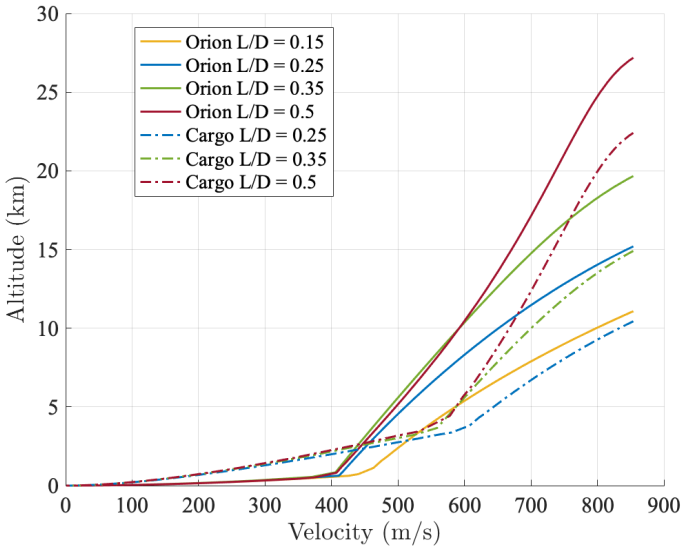

Figure 12: Altitude Vs Velocity during EDL for powered descent

The simulation was run for the nominal Orion (L/D = 0.15) and nominal Cargo vehicle (L/D = 0.25) for the different SRP systems, shown in Figure 13. There was little difference between velocity, altitude, flight path angle or throttling for the different engines. The primary difference was in the change in mass during powered descent. The higher I_sp LOX-Methane system does result in a higher landed mass, preserving 9130kg landed mass for Orion, compared to the 8555kg preserved by the SpaceX SuperDraco system, and preserving 33,888kg landed mass for the Cargo EV compared to 31,183 kg for the SuperDraco. So future EDL systems for Mars should endeavour to use a higher Isp fuel.

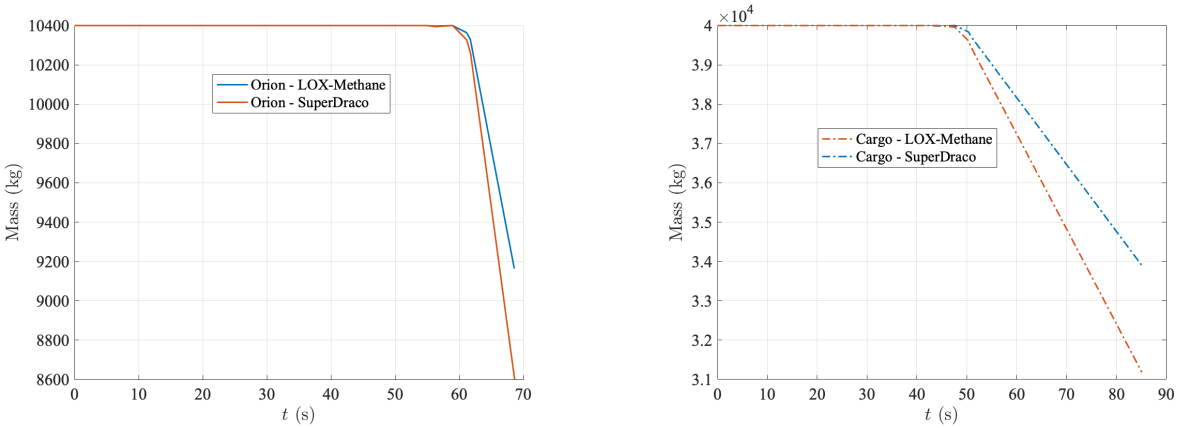

Figure 13: Mass change for Orion (*left*) and Cargo (*right*) during EDL for powered descent for different SRP engines

7.3 Two Phase - Bank Control and Powered Descent

The two phase problem was formulated with the following bounds and initial and terminal values.

Table 10: Initial and Terminal Conditions for Two Phase Descent

Variable	P1: Initial	P1: Final	P2: Initial	P2: Final
Time (s)	0	free	free	free
Altitude (km)	125	free	free	0
Velocity (km/s)	3.36	Mach 1 - Mach 6	Mach 1 - Mach 6	free
Flight Path Angle (°)	-15	free	free	free
Downrange Distance (km)	0	free	free	free
Bank Angle (°)	free	free	free	free
Mass (kg)	10,400, 40,000	10,400, 40,000	10,400, 40,000	free

Table 11: Flight Parameter Bounds for Two Phase Descent

Variable	P1: Lower	P1: Upper	P2: Lower	P2: Upper
Time (s)	0	5000	0	5000
Altitude (km)	10	125	0	125
Velocity (km/s)	0	7.5	0	7.5
Flight Path Angle (°)	-25	25	-90	90
Downrange Distance (km)	-1.00E6	1.00E6	-1.00E6	1.00E6
Bank Angle (°)	0	180	0	0
Mass (kg)	10,400, 40,000	10,400, 40,000	0	10,400
Throttle	N/A	N/A	0	1
G-Loading	0	4.5	0	4.5
Heat-Rate (W/cm^2)	0	100	0	100

In order to make the solution converge, the bounds for the initial state for Phase 2 were set slightly wider than the bounds for the terminal state in Phase 1. Path constraints for G-loading and convective heat-rate were enforced. Unfortunately, an optimal solution for the problem could not be found however acceptable solutions were reached in all cases. Further examination of the code is required to determine why an optimal solution could nto be reached, as an optimal solution was possible in both of the single pahse cases.

In examining the relative error in each phase, the 1st phase converged with very small maximum relative error in the mesh (<1.00E-6) however the second phase would fail to satisfy the error tolerance of 1.00E-4. Examination of the acceptable solutions generated still gives insight into the feasibility of such a control scheme for Mars EDL and the landed masses possible. The results of the simulation are shown below. The first set of plots is the nominal case for the Orion vehicle (L/D = 0.15) in order to clearly see the phase change, control scheme and mass changes.

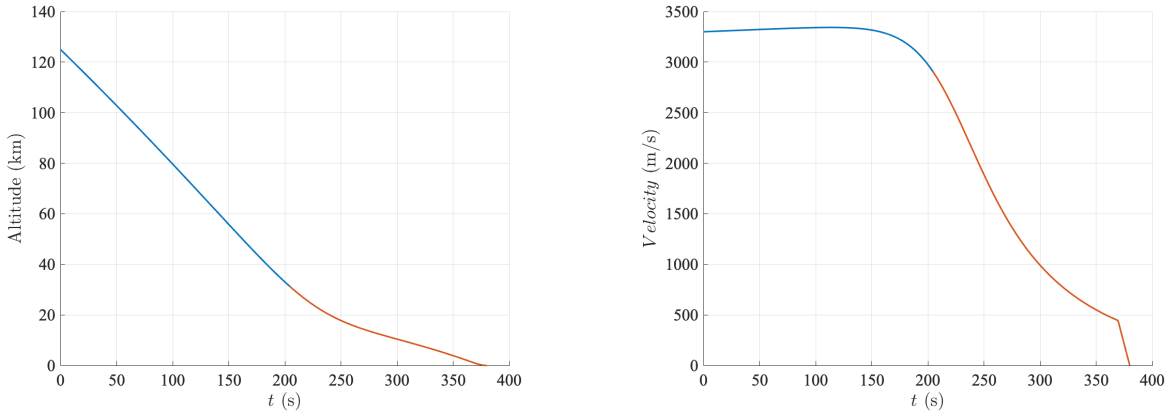

Figure 14: Altitude (*left*) and velocity (*right*) during EDL with Bank and Throttle Control for Orion EV, L/D = 0.15. Phase 1 is shown in blue, phase 2 in red.

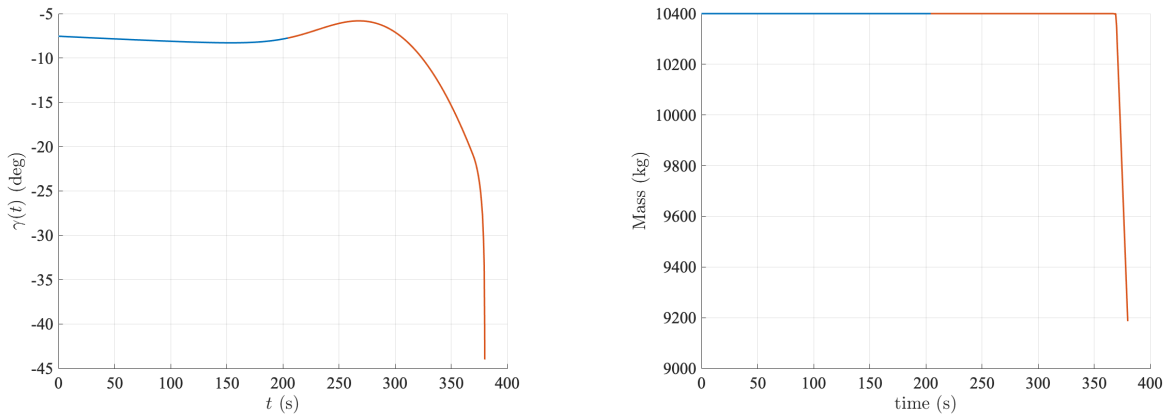

Figure 15: Flight Path Angle (left) during EDL, and Mass (*right*) during EDL with Throttle Control for Orion EV, L/D = 0.15. Phase 1 is shown in blue, phase 2 in red

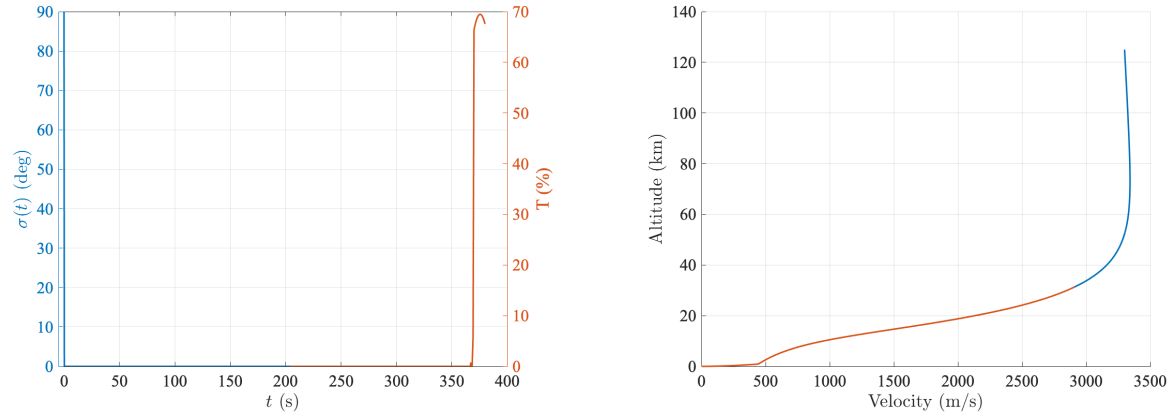

Figure 16: Optimal Bank and Throttle Control *(left)*, and Altitude vs Velocity *(right)* during EDL for powered descent for Orion EV, L/D = 0.15. Phase 1 is shown in blue, phase 2 in red

Initially, in order to ensure SRPs wouldn't be ignited outside of the SRP window, the final velocity of Phase 1 and the initial velocity of Phase 2 were set to bounds [Mach 1, Mach 6], the current range over which SRP systems have been simulated.[2] However these constraints made it difficult to find a solution and so they were removed. These constraints proved to be unnecessary as can be seen in Figure 11, while the second phase begins well above Mach 6, the SRPs do not begin firing until the velocity is approximately Mach 2, indicated by the sharp decline in velocity on the graph. The acceptable solution follows the expected trajectory found in the two single phase problems. The bank angle shifts immediately to a lift-up configuration and holds that position until the end of Phase 1. As there is no bank angle control in Phase 2, the entry vehicle is still in the lift up configuration throughout Phase 2. The EV continues to freefall towards the surface, maximising the deceleration effect of atmospheric drag prior to SRP ignition. SRP ignition occurs approximately 370 seconds into the EDL maneouvre. To avoid exceeding G-loading constraints, the engines are only throttled up to 70%, and then throttled back slightly to avoid high G-loading.

Using the hypothetical LOX-Methane engines, the landed mass on the surface of Mars with an Orion vehicle (L/D = 0.15) is 9077kg. Using the propellant mass fraction (PMF) equation

$$PMF = 1 - \frac{m_f}{m_0} \tag{32}$$

we find that this trajectory, entering at a speed of 3.36 km/s, utilising throttle and bank

control, supports a PMF of 12%. Taking into account the weight of the theoretical SRP system this still leaves a significant amount of landed mass for crew and crew systems.

Figures 17 to 21 look at different cases of β (Orion EV and Cargo EV) and L/D.

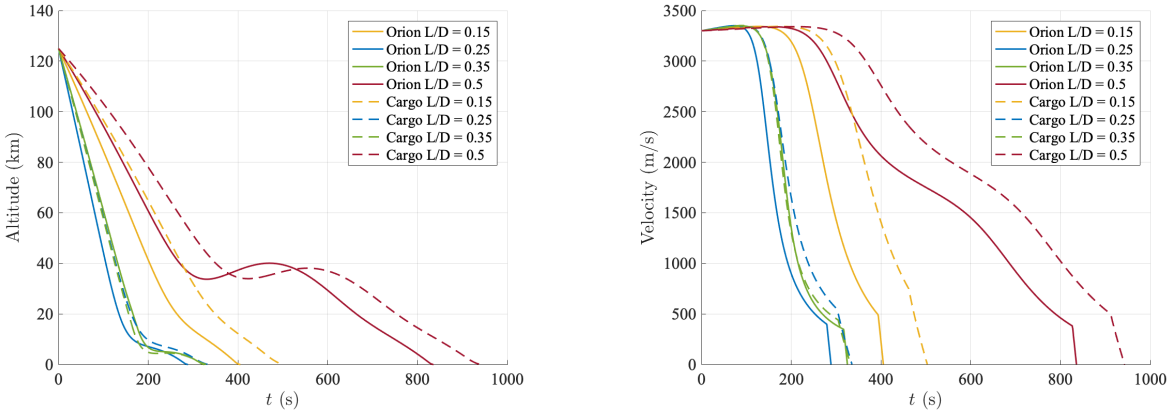

Figure 17: Altitude (*left*) and velocity (*right*) during EDL with Bank and Throttle Control for different EV and L/D.

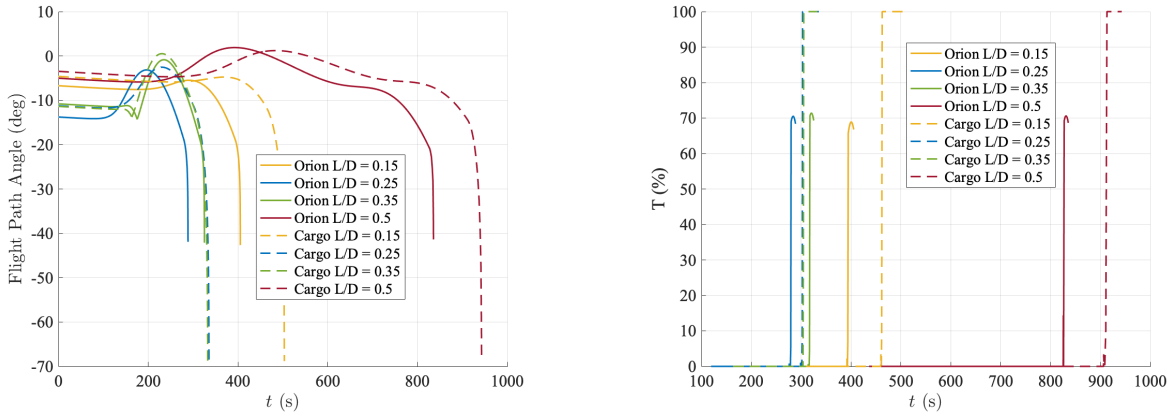

Figure 18: Flight Path Angle (left) during EDL, and Thrust (*right*) during EDL with Bank and Throttle Control for for different EV and L/D.

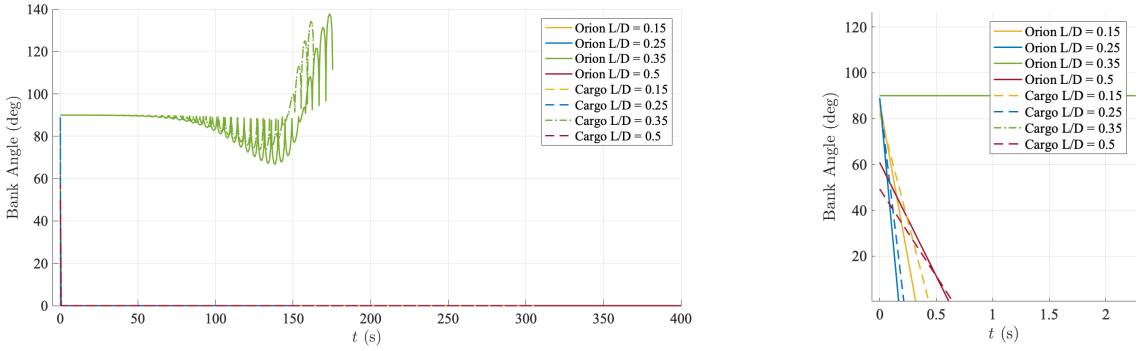

Figure 19: Optimal Bank Control *(left)*, and zoomed in early Bank Control *(right)* during EDL for powered descent for different EV and L/D.

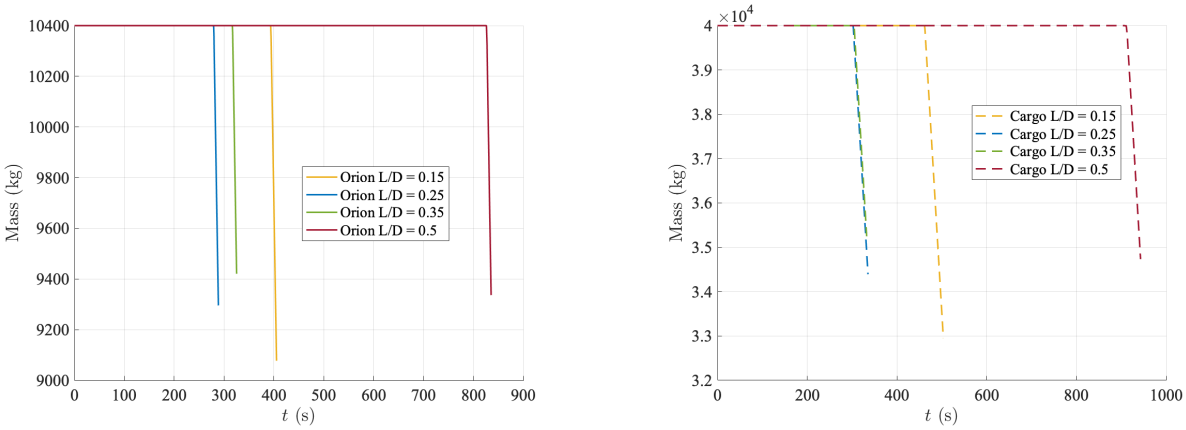

Figure 20: Mass changes for Orion *(left)*, and Cargo EV *(right)* during EDL for powered descent for different L/D.

From these figures it is evident that β and L/D have an impact on the control scheme. As was seen in the single phase case, the higher L/D craft delecerate at a slower rate through the atmosphere and change altitude at a slower pace. The lower β craft, i.e. the Orion capsule, only throttles to a thrust of 70% when throttling up the SRPs, compared to 100% throttle for the Cargo vehicle, due to the Cargo vehicle's higher β. As L/D increases, so does the ignition time of the SRPs. The higher L/D is being utilised by the craft to slow the craft without the need for throttle, thereby minimizing the mass of propellant used. The bank angle control is similar in all cases except for both the Cargo and Orion EV L/D = 0.35. In all other cases, the bank angle is quickly shifted into a full lift-up configuration to maximise L/D on descent. For the L/D = 0.35 case, we see signficicant oscillations in the bank angle. This oscillations could be due to the fact the controller is not constructed as a rate controller in this simulation. Enforcing a angular rate or angular acceleration constraint on this simulation may improve the smoothness of the bank controller for higher entry speeds. It should also be included in future simulations to account for rotational acceleration loads on the EV astronauts.

In both the Orion and Cargo EV, the lower L/D results in a lower mass delivered to the surface. Suprisingly, the higher L/D does not yield the highest mass delivered to the surface. In both EV cases, the L/D = 0.35 case delivers a higher mass than L/D = 0.5. The results are summarized in the table below. As expected, the higher ballistic coefficient vehicle (the Cargo EV) uses a higher amount of propellant to slow down.

Entry Vehicle	β	**L/D**	**Entry Mass (kg)**	**Landed Mass (kg)**	**PMF (%)**
Orion	300	0.15	10,400	9,077	12.72
	300	0.25	10,400	9,296	10.62
	300	0.35	10,400	9,421	9.42
	300	0.5	10,400	9,337	10.23
Cargo	460	0.15	40,000	32,955	17.61
	460	0.25	40,000	34,393	14.02
	460	0.35	40,000	35,250	11.88
	460	0.5	40,000	34,734	13.17

There is a nonlinear relationship between the L/D of the vehicle and the landed mass on Mars, as shown in Figure 21. Given the strange bank control behaviour of the 0.35 case, it is unclear if the value of PMF for this case is valid. Despite this, it is evident that PMF decreases nonlinearly as L/D increases. If the 0.35 value is ignored, the effect on mass of increasing the L/D lessens as L/D increases. This suggests there is likely to be a limit to the amount L/D can be increased while still benefiting the PMF.

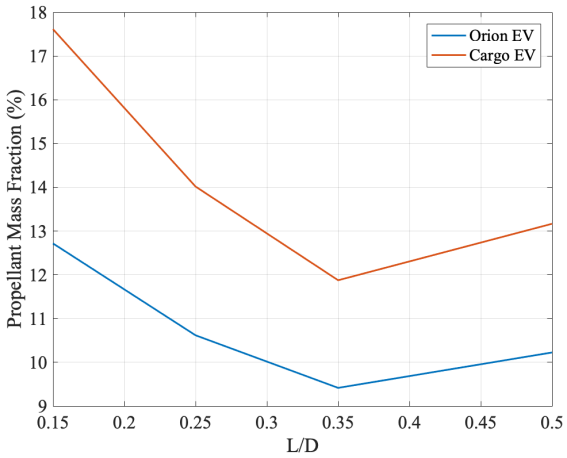

Figure 21: Propellant Mass Fraction for different Lift-To-Drag Ratios for Mars EDL with Bank and Throttle Control

In comparing these trajectories to previous Mars EDL trajectories, we see that the results closely align with previous Mars EDLs, though starting from a much lower entry velocity.

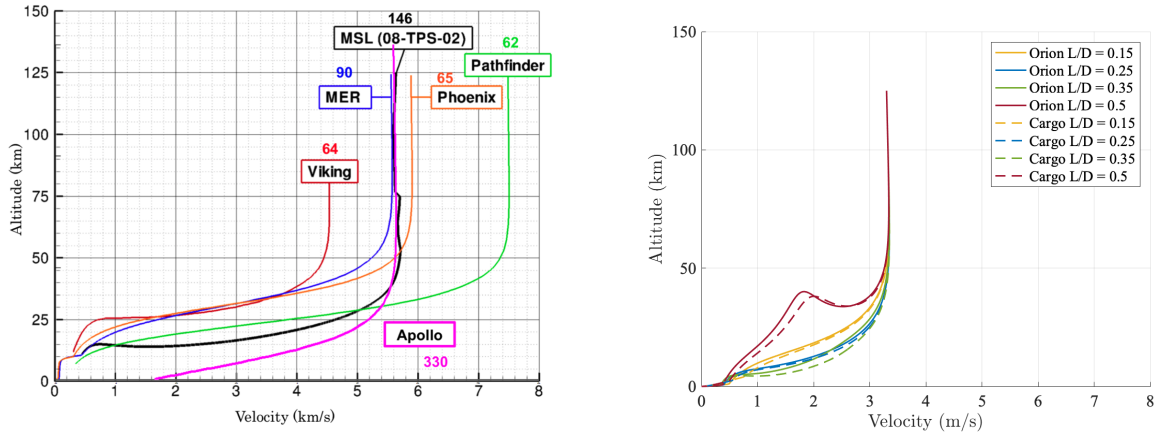

Figure 22: Comparison of past Mars EDL *(left)*[2] and the optimized two-phase problem

8 Conclusion

In conclusion, this study has demonstrated a possible control scheme for a Mars EDL trajectory that employed an unpowered bank angle phase and a powered SRP descent phase. By maneouvering the craft into a lift-up configuration for the unpowered descent phase, allowing the craft to decelerate through the atmophere, and switching on the throttle at the last possible moment, mass on the surface can be maximized. This control scheme minimizes the mass of propellant required, while still maintaining sufficiently low loading for the passengers/cargo and low convective heat rates for the aeroshell. As the mass of entry vehicles increases in the future, powered descents are a viable alternative to supersonic parachutes or subsonic propulsion. Increasing the L/D of the vehicle may have benefits in the possible landed mass achieved, however the effects of the ballistic coefficient must be taken into account. For craft with a very high ballistic coefficient, a higher propellant mass fraction will be required. Future work could invetstigate ways to lower the ballistic coefficent, such as deployable aeroshells.

References

[1] R. D. Braun and R. M. Manning. Mars exploration entry, descent, and landing challenges. *Journal of Spacecraft and Rockets*, 44(2):310–323, 2007.

[2] M. H. Fagin. Payload mass improvements for supersonic retropropulsive human class missions to mars. Master's thesis, Purdue University, Western Lafayette, Indiana, 2015.

[3] B.G. Drake. Human exploration of mars design reference architecture 5.0. Technical Report NASA/SP-2009-566, National Aeronautics and Space Administration, NASA Johnson Space Center, Houston, TX, 2009.

[4] M. A. Patterson and A. R. Rao. GPOPS-II-Next=Generation Optimal Control Softwar. Software Package, Ver. 2.1.3, RP Optimization Research, LLC, Gainsville, FL, 2013.

[5] M. Schoenemberger, A. Dyakonov, W. Scallion, and J. Van Norman. Aerodynamic challenges for the mars science laboratory entry, descent and landing. In *41st AIAA Thermophysics Conference*, volume no. AIAA 2009-3914, pages 1–29, June 2009.

[6] Marsh C. and Braun R. D. Fully-propulsive mars atmospheric transit strategies for high-mass missions. *Journal of Spacecraft and Rockets*, 48(2):271–282, 2011.

[7] Mall K. and Grant M. J. High mass mars exploration using slender entry vehicles. In *AIAA Atmospheric Flight Mechanics Conference*, San Diego, CA, January 2016.

[8] C. G. Lorenz and Z. R. Putnam. Entry Trajectory Options for High Ballistic Coeffcient Vehicles at Mars. *Journal of Spacecraft and Rockets*, 56(3):811–822, 2019.

[9] K. Sutton and R. A. Graves. A general stagnation-point convective-heating equation for arbitrary gas mixtures. Technical Report NASA TR R-376, National Aeronautics and Space Administration, NASA Langley Research Center, Hampton, VA, 1971.

[10] K. J. Murphy, K L Bibb, G J Brauckmann, M N Rhodes, B Owens, D T Chan, E L Walker, J H Bell, and T M Wilson. Orion crew module aerodynamic testing. In *29th AIAA Applied Aerodynamics Conference*, Honolulu, HI, 2011.

[11] D R Williams. Mars fact sheet. `http://nssdc.gsfc.nasa.gov/planetary/factsheet/marsfact.html`. Accessed 2 May 2020.

[12] A M Korzun, G F Dubosa, C K Iwata, B A Stahl, and J J Quicksall. A concept for the entry, descent, and landing of high mas payloads at mars. *Acta Astronautica*, 66(7):1146–1159, 2010.

[13] M.A. Tigges, B. D. Bihari, J.P. Stephens, G. A. Vos, K. D. Bilimoria, E.R. Mueller, H. Law, W. Johnson, R.E. Bailey, and B. Jackson. Orion capsule handling qualities for atmospheric entry. In *AIAA Guidance, Navigation, and Control Conference, Portland, Oregon*, August 2011.

[14] K.T. Edquist, A. M. Korzun, A. A. Dyakonov, J. W. Studak, D. M. Kipp, and I. C. Dupzyk. Development of supersonnic retropropulsion for future mars, entry, descent, and landing systems. *Journal of Spacecraft and Rockets*, 51(3):650–663, 2014.